Petrofabric derived seismic properties of a mylonitic quartz simple shear zone: implications for seismic reflection profiling

GEOFFREY E. LLOYD AND J-MICHAEL KENDALL

School of Earth Sciences, The University, Leeds LS2 9JT, UK
(email: g.lloyd@earth.leeds.ac.uk)

Abstract: The link between petrofabric (LPO) and seismic properties of an amphibolite facies quartzo-feldspathic shear zone is explored using SEM/EBSD. The shear zone LPO develops by a combination of slip systems and dauphine twinning with ***a***-maximum parallel to lineation (X) and ***c***-maximum normal to mylonitic foliation (XY). The LPO are used to predict elastic parameters from which the three dimensional seismic properties of different shear zone regions are derived. Results suggest that LPO evolution is reflected in the seismic properties but the precise impact is not simple. In general, the P-wave velocity (Vp) minimum is parallel to the ***a***-axis maximum, the direction of maximum shear wave splitting (AVs) is parallel to mylonitic foliation and the Vp maximum and AVs minimum are parallel to the ***c***-axis maximum. The seismic anisotropy predicted is significant and increases from shear zone wall rock to mature mylonite. P-wave anisotropy ranges from 11-13%, fast and slow shear waves anisotropy range from 6-15% and the magnitude of shear wave splitting ranges from 9-16%. Nevertheless, such anisotropy requires a considerable thickness of rock with this LPO before it becomes seismically visible (i.e. 100's m for local earthquakes, 10's m for controlled source experiments). However, reflections and mode conversions provide much better resolution, particularly across tectonic boundaries. The low symmetry and strong anisotropy due to the LPO suggest that multi-azimuth wide-angle reflection data may be useful in the determination of the deformation characteristics of deep shear zones.

A number of factors may produce elastic anisotropy in rocks, including variations in the spatial distribution of mineral phases, layering, grain size and shape fabrics, grain boundary properties and the presence of oriented pores or fractures (e.g., Kern & Wenk 1985; Mainprice et al. 2003). In addition, because elastic properties vary with respect to direction in single crystals, the majority of rock-forming minerals are elastically anisotropic (e.g. Christensen 1966). Thus, deformation processes, such as dislocation creep, which produce strong crystal lattice preferred orientations (LPO) in anisotropic minerals, may also induce bulk elastic anisotropy. It is no surprise therefore that petrophysical properties, such as seismic velocities, are often highly anisotropic in bulk rock aggregates (e.g. Babuska & Cara 1991).

Understanding of the impact of microstructural variables on elastic anisotropy has been obtained typically from experimental measurements of elastic properties of minerals or theoretical models that incorporate microstructural variables (e.g. Burlini & Kern 1994; Wendt et al. 2003). Experimental studies have focused primarily on the influence of fractures or LPO on the elastic properties of minerals and rocks. In particular, the seismic properties can be measured via direct laboratory methods at ambient or elevated temperatures and pressures (e.g. Kern 1982), although it is often difficult or impossible to obtain the complete three dimensional property orientation distribution from a single experiment (however, see Pros et al. 2003). Furthermore, experimental investigation of seismic properties usually involves rocks in which all microstructural fabric elements contribute, effectively masking any LPO component.

An alternative approach is to calculate the seismic properties of a rock aggregate from individual crystal orientation measurements, incorporating the single crystal elastic constants and the LPO for each mineral weighted according to its modal content (e.g. Mainprice & Humbert 1994). The seismic phase velocities and anisotropies then can be calculated in every direction (e.g. Mainprice & Silver 1993). Recently, the advent of electron backscattered diffraction (EBSD) in the scanning electron microscope (SEM) has made it possible to measure LPO in statistically viable numbers from different minerals within a rock aggregate whilst maintaining a one-to-one relationship with other microstructural elements (e.g. Mainprice et al. 1993, Lloyd 2000; Mauler et al. 2000; Bascou et al. 2001). In this contribution, the seismic properties of an amphibolite facies, mylonitic quartz shear zone are predicted by averaging the single crystal elastic properties according to the SEM/EBSD derived LPO in order to study the relationship between microstructure, petrofabric and seismic properties. This approach illustrates the usefulness of integrating geological studies of rock microstructures, and particularly petrofabrics, with geophysical studies of seismic properties to obtain a fuller understanding of geodynamic processes.

Specimen details

The sample used in this study was collected from a 30cm wide deformed planar quartz vein (Fig. 1a)

within Proterozoic gneisses at the head of Upper Loch Torridon, NW Scotland (UK GR NG 840530; Wheeler 1984). It seems to have deformed by bulk simple shear and has been described in detail previously (Law et al. 1990; Lloyd et al. 1992; Lloyd *in press*). The salient aspects of these studies

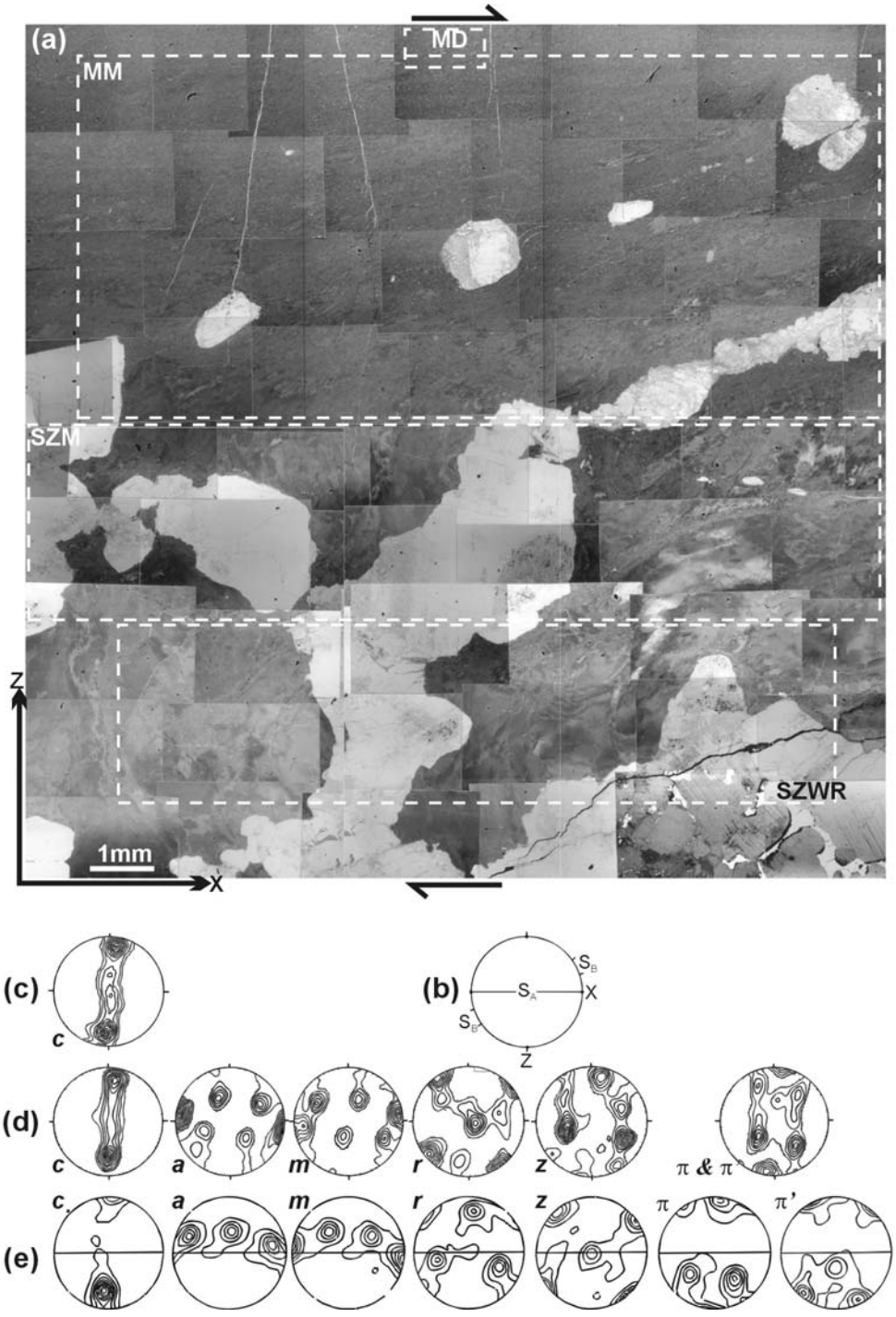

Fig. 1. Summary of Torridon simple shear zone microstructure and LPO. All pole figures equal area, upper hemispheres viewed towards ENE; contour intervals multiples of mean uniform distribution. (a) SEM electron channelling (see Lloyd 1987 for details) orientation contrast image of microstructure, indicating positions of SEM/EBSD analyses: SZWR, shear zone wall rock (analysis G 030600); SZM, shear zone margin (G040800); MM, mature mylonite (G270700); and MD, mylonite/shear zone detail (G050800). Amended from Lloyd (*in press*). (b) Specimen co-ordinates for all LPO diagrams (after Law et al. 1991). (c) Universal stage optical ***c***-axis pole figure; 1815 measurements (after Law et al. 1991). (d) X-ray pole figures for ***c, m, a, r, z*** and $\boldsymbol{\pi + \pi'}$ orientations (after Law et al. 1991). (e) Manual SEM electron channelling pole figures for ***c, m, a, r, z,*** $\boldsymbol{\pi}$ and $\boldsymbol{\pi'}$ orientations after Lloyd et al. 1992)

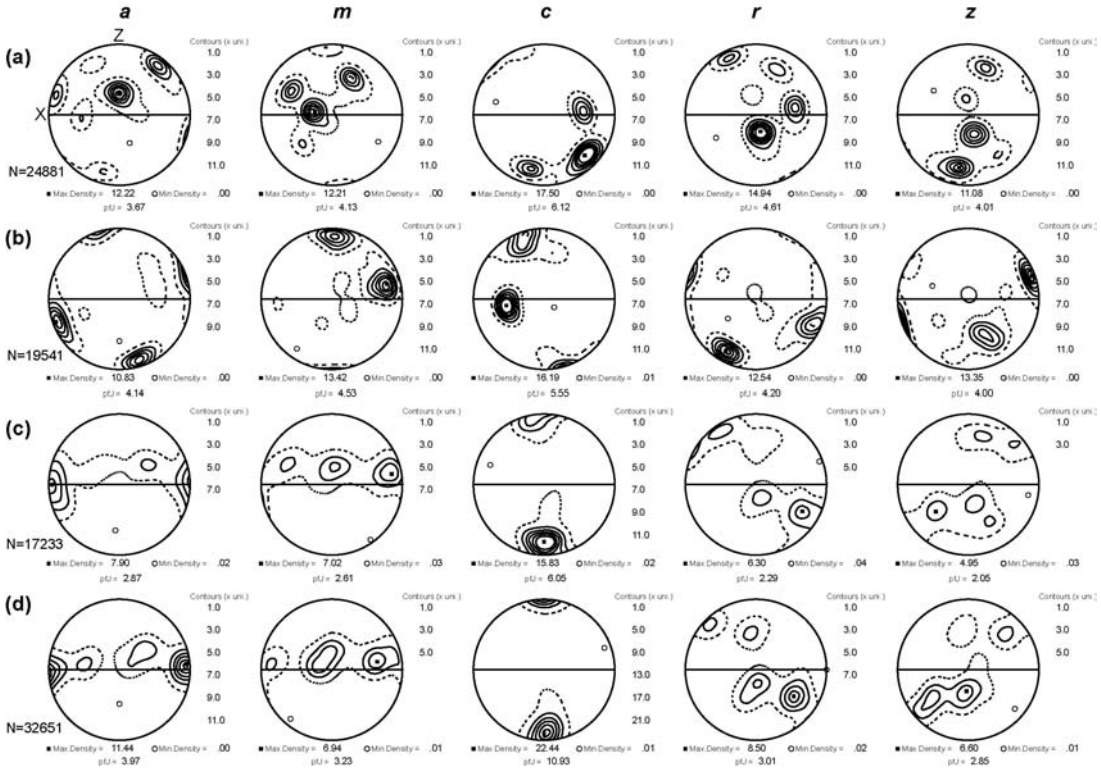

Fig. 2. Summary (after Lloyd, *in press*) of SEM/EBSD pole figures for ***c, m, a, r*** and ***z*** orientations using the program Pf2k (D. Mainprice). Only wall rock includes quartz and plagioclase, the rest involve quartz alone. All pole figures equal area, upper hemispheres viewed towards ENE; contours multiples of mean uniform distribution, as indicated (pfJ is an indication of distribution strength, with pfJ = 1 for random; see Bunge 1982). (a) Shear zone wall rock (SZWR). (b) Shear zone margin (SZM). (c) Mature mylonite (MM). (d) Mylonite details (MD).

relevant to the present contribution are as follows.

The vein was deformed by crystal plastic processes to form a dextral shear zone with an intense mylonitic foliation and lineation (Fig. 1a, region MM). The foliation locally displays the orientation variations expected for heterogeneous simple shear (e.g. Ramsay & Graham 1970; Ramsay 1980): X parallel to lineation, XY parallel to foliation and Z normal to foliation. The shear zone wall rock (Fig. 1a) comprises coarsely crystalline quartz and plagioclase feldspar. Foliation at the shear zone margins (Fig. 1a) is oriented at ~45° to the vein walls but curves rapidly with a dextral shear sense to become sub-parallel to the walls. In the XZ section analysed in this contribution, the vein microstructure is that of a classic Type II S-C mylonite (Lister & Snoke 1984) and consists of two planar domains, A (grain size <5μm) and B (grain size <100μm), aligned parallel to the macroscopic mylonitic foliation (S_A). The obliquity between grain axes (S_A, S_B) in the two domains is consistent and indicates a dextral shear sense. The microstructures observed are indicative of constant volume, strongly non-coaxial, essentially plane strain deformation that closely approximates to simple shear.

The quartz petrofabric (Figs. 1c-e and 2) is characterized by an <***a***> axis maximum sub-parallel to X, which occupies a pole position to the corresponding single girdle (***c***) axis fabric, with a (***c***) axis maximum oriented sub-normal to the XY foliation plane and normal to the average of the quartz basal plane defined by the LPO. These associations suggest a simple relationship between shear zone geometry, simple shear kinematic framework and orientation of crystal slip systems responsible for shear zone formation. Most quartz grains are preferentially oriented to exploit slip on systems that utilise <***a***> as the slip direction (such as {***-π***}<***a***>, {***z***}<***a***>. (***c***)<***a***> and {***m***}<***a***>). Such observations can be interpreted in terms of a lower resistance to slip on negative forms compared to positive forms and/or the occurrence of significant dauphine twinning. The latter is consistent also with the {***r***} point maximum position within the XZ plane at ~35° to the foliation, subparallel to the NW-SE trending maximum principle stress direction inferred from the simple shear kinematic framework (e.g. Tullis & Tullis 1972). The petrofabric therefore approximates that of a 'dauphine twinned single crystal'.

SEM studies of the Torridon shear zone have focused attention on to the misorientations between adjacent grains and hence upon the grain boundary

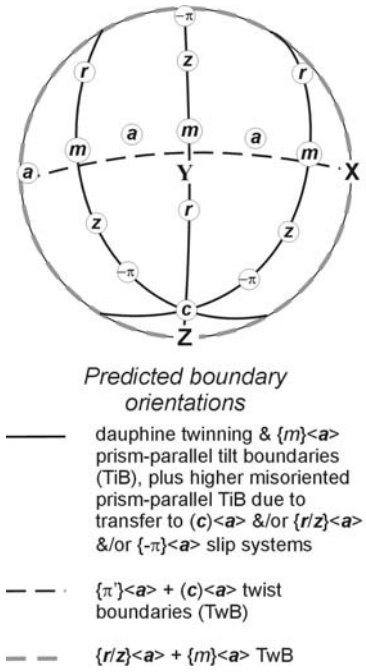

Fig. 3. Relationship between grain boundary types and orientations, and shear zone tectonic (XYZ) and crystal (<***a***>, (***c***), {***m***}, {***r***} and {***z***}) frameworks (after Lloyd, *in press*).

network, as well as the conventional grain microstructure and petrofabric. Misorientations develop by a combination of crystal slip and dauphine twinning and result in a microstructure dominated by misorientations about the (***c***) axis. Due to crystal symmetry restrictions, misorientation angles greater than 60º about the (***c***) axis are accommodated apparently by transfer of slip on to systems capable of progressively higher misorientations up to the maximum of 104.5º (i.e. successively from {***m***}<***a***>, {***r/z***}<***a***>, {***-π***}<***a***> to (**c**) <***a***>). The resulting grain boundary network (Fig. 3) consists of tilt boundaries parallel to prism (and hence often YZ tectonic) planes. Although no other tilt boundaries are formed, the individual slip systems can operate also in simple combinations to produce twist boundaries typically parallel to the XY foliation/basal crystal planes and/or XZ tectonic plane.

Methodology

LPO determination

SEM/EBSD (e.g. Venables & Harland 1973; Dingley 1984) provides the precise crystallographic orientation at the point of incidence of the electron beam on the sample surface, with a spatial resolution of ~1μm and angular resolution of ~1º (e.g. Prior et al. 1999). A one-to-one correlation is achieved therefore between crystal orientation and microstructural position. The crystal orientation is defined by three spherical Euler angles (ϕ_1, φ, ϕ_2) with respect to the sample reference frame (Bunge 1982). EBSD analysis can be performed either manually or automatically, but in both cases the diffraction patterns are indexed via computer programs; the system used in this study was the HKL Technology *Channel 5* software (e.g. Schmidt & Olesen 1989). Automated EBSD

Table 2. *Seismic properties analysis for single crystal quartz (left) and plagioclase (right)*

Quartz	Plagioclase
(a) Input crystallographic parameters	
Symmetry:	
trigonal, space group P3221	triclinic, space group P-1
Unit cell dimensions (Å) :	
a = 4.9130, b = 4.9130, c = 5.5040	a = 8.1553, b = 12.8206, c = 7.1397
Unit cell angles (degrees):	
$\alpha = 90.0$, $\beta = 90.0$, $\gamma = 120.0$	$\alpha = 93.95$, $\beta = 116.47$, $\gamma = 89.62$
Euler angle triplet:	
$\phi_{1\text{-max}} = 180°$, $\varphi_{max} = 180°$, $\phi_{2\text{-max}} = 120°$	$\phi_{1\text{-max}} = 360°$, $\varphi_{max} = 180°$, $\phi_{2\text{-max}} = 360°$

(b) Input single crystal density & elastic stiffness matrix, C_{ij} (Mbars)

density = 2.6473 g.cm^{-3}	*density* = 2.6100 g.cm^{-3}
McSkimin et al. (1965)	Aleksandrov et al. (1974)

.8680	.0704	.1191	-.1804	.0001	.0001	.8200	.3980	.4100	.0001	-.0840	.0001
.0704	.8680	.1191	.1804	.0001	.0001	.3980	1.4500	.3370	.0001	-.0630	.0001
.1191	.1191	1.0575	.0001	.0001	.0001	.4100	.3370	1.3280	.0001	-.1870	.0001
-.1804	.1804	.0001	.5820	.0001	.0001	.0001	.0001	.0001	.1810	.0001	-.0100
.0001	.0001	.0001	.0001	.5820	-.1804	-.0840	-.0630	-.1870	.0001	.3100	.0001
.0001	.0001	.0001	.0001	-.1804	.3988	.0001	.0001	.0001	-.0100	.0001	.3350

analysis enables very large (i.e. $>10^6$) orientation data sets to be acquired from samples >10x10mm area, which can be used to test and/or interpret seismic anisotropy (e.g. Burlini & Kunze 2000; Lloyd 2000; Mauler et al. 2000).

Three overlapping large-scale auto-EBSD analyses (G030100, G040800, G270700) were performed extending from the shear zone wall rock to the mature mylonite and a detailed auto-EBSD analysis (G050800) of the mature mylonite (Lloyd *in press*; see Fig. 1a for locations and Table 1 for experimental details). The LPO derived from the SEM/EBSD experiments (Fig. 2) provide a part of the input data for the seismic properties determinations described below. Important aspects of the LPO are as follows. (1) The shear zone wall rock (Fig. 2a) and shear zone margin (Fig. 2b) comprise relatively few, large quartz (and plagioclase in the former) grains and hence their LPO consist of isolated concentrations associated with individual grain orientations. (2) The mylonite LPO (Fig. 2c, d) approximates that of a 'dauphine twinned single crystal', consistent with results derived from other methods (e.g. Fig. 1c-e), which maintains (strengthens?) the <***a***>, (***c***) and {***m***} positions but interchanges the {***r***} and {***z***} positions. (3) The differences between LPO from the shear zone margin and mature mylonite indicate a rapid migration of wall rock crystal pole directions towards the mature mylonite LPO, in agreement with microstructural observations (see Fig. 1a). (4) The shear zone shear strain gradient and dynamic recrystallisation rates therefore are expected to have been steep and/or rapid.

Seismic properties determination

The propagation of seismic waves generates a short-term deformation in a medium, such that the velocity and polarisation direction of the waves depend on the elastic parameters (i.e. the elastic stiffness matrix) of the medium and the nature of the deformation. Thus, knowledge of the elastic parameters can be used to predict seismic velocities and propagation directions. The general relationship between elastic parameters and seismic waves is given by (e.g. Nye 1957, Kendall 2000),

$$(C_{ijkl} X_i X_j - \delta_{kl} \rho V^2) U_\ell = 0 , \qquad (1)$$

where C_{ijkl} is the fourth-order proportionality tensor that relates stress to strain, X_i expresses the propagation direction of the wave ($C_{ijkl}X_iX_j$ is the 3x3 Christoffel matrix), δ_{kl} is the Kronecker delta, ρ is the density of the medium, V is the phase velocity of the wave in a given direction and U_ℓ is the displacement.

A non-trivial solution for U_ℓ requires that the determinant of the system in (1) vanishes and results in the Christoffel equation (e.g. Nye 1957),

$$\det\left| C_{ijkl} X_i X_j - \delta_{kl} \rho V^2 \right| = 0 . \qquad (2)$$

The Christoffel equation has three possible solutions representing one compressional (P) and two shear (S_1, S_2) waves. Due to the symmetry of the elastic tensor, the Christoffel matrix is symmetrical also, which means that the three solutions have mutually perpendicular displacement vectors. In isotropic media, seismic wave velocities are independent of their propagation direction and their polarisation depends only on the type of wave and the nature of the source. In anisotropic media, seismic velocities depend locally on the propagation direction and their polarisation depends not only on the type of wave but also on the local symmetry of the elastic properties (i.e. C_{ijkl})

Although C_{ijkl} has 81 components, these can be reduced to a symmetrical 6 x 6 matrix, C_{ij}, because of symmetry in the stress and strain matrices (Babuska & Cara 1991). Consideration of the energy function of a strained crystal, which depends only on the strain components, reduces the stiffness matrix to a maximum of 21 *independent* coefficients. Furthermore, elastic parameters of crystalline media depend ultimately on chemical composition and atomic arrangement of the crystal structure and hence are characteristic for each mineral. Thus, the elastic parameters are closely related to the strength of interatomic bonds in corresponding directions of the crystal structure (e.g. elastic moduli are larger in the direction in which the structure has the strongest bonds). Consequently, because elastic parameters are the same in crystal symmetry related directions, the number of independent elastic coefficients for single crystals can be reduced further still depending on crystal symmetry (see Babuska & Cara 1991, table 2.1).

Single crystal seismic properties

Understanding the seismic behaviour of the individual constituent crystals is critical to any interpretation of whole rock seismic behaviour, as exhibited for example in mylonitic shear zones. As an example of the impact of crystal structure on seismic properties and the methodology used to predict whole rock seismic properties, the variations in compressional and shear waves velocities with direction have been calculated for quartz and plagioclase single crystals, the minerals of interest in the Torridon shear zone.

Figure 4a shows common morphological single crystal forms of quartz and plagioclase and their relationship to directions of maximum and minimum seismic velocities (V) and anisotropy (A), based on experimentally determined values

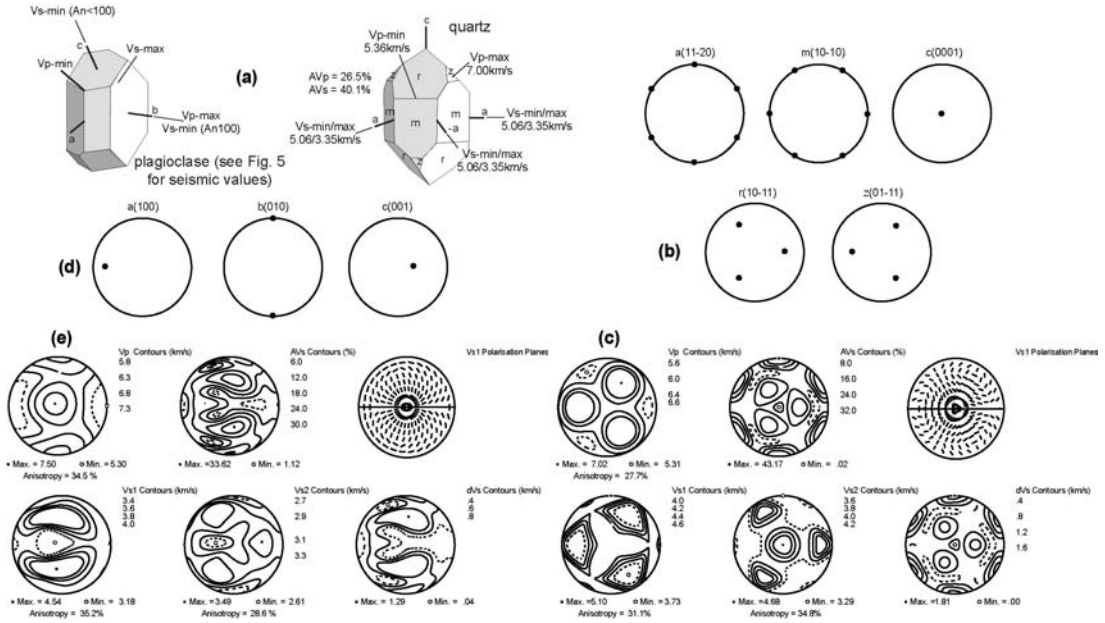

Figure 4. Seismic property distributions (Vp, Vs1, Vs2, AVs, dVs, Vs1 polarisation planes – see text for details) of quartz and plagioclase single crystals based on LPO-averaging (see Table 2 for input data). All pole figures equal area, upper hemispheres projections; contours multiples of mean uniform distribution, as indicated. (a) Quartz and plagioclase single crystal forms (after Dana & Ford, 1951) and seismic property variations (after Babuska & Cara 1991). (b) Quartz single crystal LPO generated from an individual Euler angle triplet. (c) Variation in quartz single crystal seismic properties with crystal direction. (d) Plagioclase single crystal LPO generated from an individual Euler angle triplet. (e) Variation in plagioclase single crystal seismic properties with crystal direction.

summarized by Babuska & Cara (1991). Although the principal crystal directions for quartz (i.e. $\boldsymbol{a}(11\bar{2}0)$, $\boldsymbol{m}(1\bar{1}00)$, $\boldsymbol{c}(0001)$, $\boldsymbol{r}(10\bar{1}1)$, $\boldsymbol{z}(01\bar{1}1)$) and plagioclase (i.e. $\boldsymbol{a}(100)$, $\boldsymbol{b}(010)$, $\boldsymbol{c}(001)$) can be represented on a single stereographic projection, petrofabric analysis typically plots individual 'pole figures' for each form. Appropriate Euler angle triplets (e.g. Casey 1981) for quartz and plagioclase (Table 2a) were used therefore to calculate individual pole figure diagrams (Fig. 4b, d) representative of the single crystal forms via the program *Pfch5* (Mainprice, 2003).

The single crystal elastic tensor, C_{ijkl}, is generally defined in the crystal reference frame, whereas crystal orientations are generally defined via the Euler angles in the specimen reference fame. The former can be rotated in to the latter via (Babuska & Cara 1991),

$$C_{ijkl}(g) = g_{im} g_{jn} g_{ko} g_{lp} C^{0}_{mnop}, \qquad (3)$$

where $g_{ij} = g[\phi_1, \varphi, \phi_2]$ is the crystal to sample reference frame rotation matrix and C^{0}_{mnop} is the single crystal elastic stiffness tensor in the crystallographic reference frame.

The single crystal orientations, as defined by the Euler angle triplets in (3), were combined via (2) with the experimentally determined single crystal elastic stiffness matrix and density for each mineral (i.e. quartz, McSkimin et al. 1965; plagioclase, Aleksandrov et al. 1974; see Table 2b) to calculate the single crystal seismic property distributions using the program *ANISch5* (Mainprice 2003; see also Mainprice 1990; Mainprice & Humbert 1994). Stereographic projections (Fig. 4c, e) of the seismic properties have been plotted in sample coordinates via the program VpG (Mainprice 2003). The specific property distributions calculated are the compressional (Vp) and shear (Vs1, Vs2) wave phase velocities and the degree of shear wave splitting for a given direction, represented as either the absolute difference in shear wave velocities (dVs = Vs1 – Vs2) or the shear wave anisotropy (AVs), which is conventionally calculated via (e.g. Mainprice & Silver 1993),

$$AVs\% = 100(Vs1 - Vs2)/[(Vs1 + Vs2)0.5]. \quad (4)$$

In addition, the absolute anisotropy of Vp, Vs1 and Vs2 have been calculated by substituting their appropriate maximum and minimum values for Vs1 and Vs2 respectively in (4). Finally, as shear wave splitting analysis of real data estimates the degree of splitting and the orientation of the fast shear-wave for a given ray direction (e.g. Kendall 2000), the polarisations of the fast shear waves (Vs1) are also shown in stereographic projection.

The trigonal crystal symmetry of quartz is reflected in its seismic property distributions, although AVs (and dVs) also exhibit 6-fold

Table 1. *Summary of Torridon shear zone auto-EBSD experiments (see Lloyd, in press, for further details)*

DETAILS	JOB (format: username-day-month-year)			
	G030600	G040800	G270700	G050800
Specific comments	**blown filament;*	*ended by user break*	-	-
Area analysed	shear zone wall rock	shear zone margin	mature mylonite	detail of mature mylonite
Dimensions (mm)	10.0 x 13.0	17.0 x 6.0	13.5 x 7.25	1.5 x 1.0
No. data pts.	136640	120537	228825	150001
Grid step (μm)	50	25	20	1
Time (hr:min:sec.)	41:47;25	29:37:52	41:18:56	22:11:31
Index rate (sec/ebsp)	1.1	0.88	0.65	0.53
Minerals indexed	quartz and plagioclase (An16)	quartz	quartz	quartz
MAD	<1.5	<1.5	<1.5	<1.5
% Low BC	*46.6	2.2	5.1	1.3
% Low BN	0.1	13.0	0.2	2.1
% Not indexed	27.0	68.5	87.2	74.8
% Indexed	26.19	16.21	7.53	21.77
No. indexed	35789	19541	17233	32651
No. phases	2	1	1	1
Phase 1	quartz	quartz	quartz	quartz
Total good pts	24881	19541	17233	32651
Good pts %	18.21	16.21	5.53	21.77
Vol. fraction %	69.52	100.00	100.00	100.00
Phase 2	plagioclase	-	-	-
Total good pts	10908	-	-	-
Good pts %	7.98	-	-	-
Vol. fraction	30.48	-	-	-

Key: MAD, mean angular deviation; BC, band contrast; BN, band number; in all but G030100 plagioclase was ignored

symmetry close to the basal plane (Fig. 4c). Single crystal quartz is highly anisotropic in terms of all of its seismic properties. The seismic property distributions for plagioclase are more complex, reflecting the triclinic crystal symmetry, although a seismic symmetry plane normal to ***b***(010) is apparent (Fig. 4e). Single crystal plagioclase is almost as anisotropic as quartz in terms of all of its seismic properties.

Elastic parameters are known to vary with composition. It is likely therefore that seismic properties for plagioclase vary with anorthite (An) content. The experimentally determined density and elastic stiffness matrix data used to derive Fig. 4e was for plagioclase An_{16}, specifically because electron microprobe analysis of the plagioclase in the Torridon shear zone showed a composition range of $An_{15\text{-}23}$. Babuska and Cara (1991, table 3-1) have summarized experimentally measured seismic properties for four other plagioclase compositions (An_9, An_{29}, An_{53} and An_{100}). In an attempt to constrain quantitatively the variations in seismic properties with plagioclase composition, the four sets of experimental values together with the single crystal values for An_{16} derived above have been plotted in Fig. 5. The velocities vary linearly across the range of compositions, showing slight to moderate increases with An content. In contrast, both the anisotropy of Vp and shear wave splitting are almost invariant with An content.

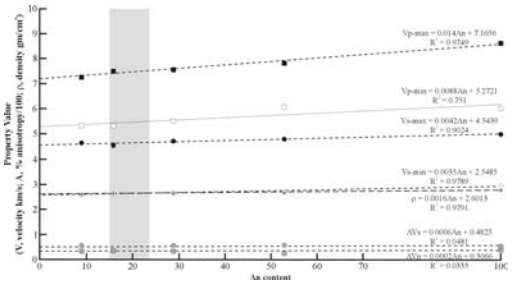

Fig. 5. Variation in seismic properties (Vp, AVp, Vs1, Vs2, AVs – see text for details) and density (ρ) with An content in plagioclase (n.b. anisotropy represented from 0 - 1 rather than 0 - 100%). Data for An_9, An_{29}, An_{53}, An_{100} from Babuska & Cara (1991); Data for An_{16} derived from LPO-averaged values using experimentally measured elastic parameters (see Table 2). Broken lines are best fit trends through and R^2 is the correlation coefficient. The shaded box indicates the range of An values measured in Torridon shear zone.

Table 3. *Summary of elastic properties (stiffness matrix) derived via LPO analysis using Voigt-Reuss-Hill (VRH) averaging*

Samples	G030600 – shear zone wall rocks	G040800 – shear zone margins	G270700 – mature mylonites	G050800 – mylonite details
Aggr. density	2.6359gm.cm-3	2.6473gm.cm-3	2.6473gm.cm-3	2.6473gm.cm-3
VRH average elastic stiffness: quartz fractions	9965 .0652 .0964 .0082 -.0241 .0248 .0652 .9789 .0952 -.0220 .0002 .0183 .0964 .0952 .9075 -.0309 -.0119 .0047 .0082 -.0220 -.0309 .4442 .0332 -.0209 -.0241 .0002 -.0119 .0332 .4579 -.0201 .0248 .0183 .0047 -.0209 -.0201 .4534	.9595 .0787 .1199 -.0305 .0231 .0185 .0787 .9304 .0875 .0461 .0353 -.0213 .1199 .0875 .9110 .0332 -.0421 .0256 -.0305 .0461 .0332 .4385 .0394 .0404 .0231 .0353 -.0421 .0394 .3040 -.0001 .0185 -.0213 .0256 .0404 -.0001 .4532	1.0520 .1011 .0805 -.0106 .0051 .0021 .1011 .8514 .1140 .0082 .0103 .0023 .0805 .1140 .9030 .0008 -.0517 .0045 -.0106 .0082 .0008 .4192 .0094 -.0114 .0051 .0103 -.0517 .0094 .4919 -.0117 .0021 .0023 .0045 -.0114 -.0117 .4876	1.0605 .1127 .0824 .0077 .0045 .0040 .1127 .8479 .1005 -.0022 .0101 .0078 .0824 .1005 .9051 -.0086 -.0614 -.0044 .0077 -.0022 -.0086 .3942 .0003 -.0178 .0045 .0101 -.0614 .0003 .4988 .0060 .0040 .0078 -.0044 -.0178 .0060 .5097
VRH average elastic stiffness: plagioclase fractions	9087 .4010 .4426 -.0315 .0479 .0430 .4010 1.1202 .4349 -.0393 .0000 .0693 .4426 .4349 .10956 -.0395 .0419 .0657 -.0315 -.0393 -.0395 .3882 .0230 -.0088 .0479 .0000 .0419 .0250 .3435 -.0086 .0430 .0693 .0657 -.0088 -.0086 .2982	n/a n/a n/a analysed n/a n/a	n/a n/a n/a analysed n/a n/a	n/a n/a n/a analysed n/a n/a
VRH average elastic stiffness: each regions	9453 .1623 .1965 -.0060 .0005 .0269 .1623 1.0062 .1863 -.0260 -.0032 .0329 .1965 .1863 .9465 -.0319 .0032 .0232 -.0060 -.0260 -.0319 .3890 .0304 -.0159 .0005 -.0032 .0032 .0304 .4191 -.0156 .0269 .0329 .0232 -.0159 -.0156 .3868	9595 .0787 .1199 -.0305 .0231 .0185 .0787 .9304 .0875 .0461 .0353 -.0213 .1199 .0875 .9110 .0332 -.0421 .0256 -.0305 .0461 .0332 .4385 .0394 .0404 .0231 .0353 -.0421 .0394 .3040 -.0001 .0185 -.0213 .0256 .0404 -.0001 .4532	1.0520 .1011 .0805 -.0106 .0051 .0021 .1011 .8514 .1140 .0082 .0103 .0023 .0805 .1140 .9030 .0008 -.0517 .0045 -.0106 .0082 .0008 .4192 .0094 -.0114 .0051 .0103 -.0517 .0094 .4919 -.0117 .0021 .0023 .0045 -.0114 -.0117 .4876	1.0605 .1127 .0824 .0077 .0045 .0040 .1127 .8479 .1005 -.0022 .0101 .0078 .0824 .1005 .9051 -.0086 -.0614 -.0044 .0077 -.0022 -.0086 .3942 .0003 -.0178 .0045 .0101 -.0614 .0003 .4988 .0060 .0040 .0078 -.0044 -.0178 .0060 .5097

Polycrystal seismic properties

Mineral grains in a rock contribute to the overall seismic properties according to their single crystal elastic parameters, crystallographic orientation distribution (LPO) and volume fraction. However, although the effect of LPO on seismic wave velocities has long been recognized (e.g. Kaarsberg, 1959; Hess, 1964), the significance of LPO on the seismic properties of rocks depends on how the seismic velocities are related to the crystal directions and the origin of the LPO. There must be a significant degree of crystal alignment to produce a seismic anisotropy, whilst randomly oriented crystals generate an isotropic bulk rock. Most LPO causing mechanisms (e.g. dislocation creep) considered in seismic studies are induced by tectonic stresses in highly deformed rocks (e.g., Babuska and Cara 1991; Blackman et al. 1996).

The methodology used to calculate polycrystal seismic property distributions is the same as that employed in the single crystal calculations described above. For each mineral grain orientation, measured via SEM/EBSD, the single crystal parameters (Table 2b) need to be rotated into the sample reference frame using (3), such that the elastic parameters of the polycrystal are derived by integration over all possible orientations in the three-dimensional orientation distribution function. The three seismic phase velocities (Vp, Vs1 and Vs2), and related anisotropy (AVp, AVs), can be obtained then in every direction via solution of (2). However, due to stress/strain compatibility assumptions, three different averaging schemes are possible. The *Voigt* (V) average (Voigt 1928) assumes a constant strain approximation, whilst the *Reuss* (R) average (Reuss 1929) assumes a constant stress approximation in calculating the compliance tensor, the inverse of the stiffness tensor (e.g. Crosson & Lin 1971). The Voigt and Reuss averages represent idealized situations and provide upper and lower bounds respectively for the real elastic parameters (Bunge et al. 2000). Thus, the mean or *Hill* (H) average (Hill 1952) of the two values is often taken as the best estimate (VRH) of the average elastic parameters.

Finally in this section, it must be emphasised that the prediction of seismic properties using the LPO averaging approach requires accurate data on single crystal elastic parameters of different minerals. Such data are usually determined by measuring the ultrasonic velocities of single crystals in different directions and deriving the elasticity tensor via the Cristoffel equation (e.g. McSkimin et al. 1965), although a more recent approach uses Brillioun scattering and is more accurate (e.g. Sinogeikin & Bass 2000). Nevertheless, relevant data for many minerals are still lacking, although the situation is rapidly improving (e.g. Ji et al. 2002). Furthermore, single crystal elastic properties vary with pressure (P) and temperature (T) but the PT-derivative values are often unavailable. Following the current convention established for mantle minerals (e.g. Mainprice et al. 2000), we assume the elastic parameters of quartz and feldspar determined under ambient conditions (McSkimin et al. 1965; Aleksandrov et al. 1974).

Table 4. *Summary of single crystal and Torridon shear zone seismic properties (see Figs. 6 and 8)*

Property		Single crystal	SZ wall rock	SZ margin	Mature mylonite	Mylonitic detail
Vp	max.	Q: // ***z***	Q: broad // ***c***	Q: broad sub-// ***c***	Q: sub-// ***c***, ***r***, ***z***	Q: sub-// ***c***, ***r***, ***z***
		P: sub-// (101)	P: broad // (001)	-	-	-
			T: broad sub-// σ_1	T: broad sub-// σ_1	T: sub-// ***Z***	T: sub-// ***Z***
	min.	Q: sub-// ***r***	Q: sub-// ***a***, ***z*** ?	Q: ?	Q: // ***a*** & basal plane	Q: // ***a*** & basal plane
		P: // (001)	P: sub-// (100)	-	-	-
			T: sub-// ***Y***, σ_3	T: sub-// ***Y***	T: // ***X***, sub-// ***XY***	T: // ***X***, sub-// ***XY***
Vs1	max.	Q: // ***a***	Q: broad sub-// ***c***, ***r***	Q: broad sub-// ***c***, ***r***	Q: // basal plane, sub-// ***c***	Q: // basal plane, sub-// ***c***
		P: sub-// (110)	P: sub-// (010)	-	-	-
			T: // σ_1, sub-// ***Y***	T: sub-// σ_1, ***Y***	T: // ***X***, ***Y***, ***Z***	T: // ***X***, ***Y***, ***Z***
	min.	Q: // z	Q: broad sub-// ***a, m*** ?	Q: ?	Q: // ***z*** small circle	Q: // ***r***, ***z*** small circle
		P: sub-// (101)	P: broad sub-// (010)	-	-	-
		-	T: ?	T: ?	T: // σ_3 ?	T: // σ_1 & σ_3 ?
Vs2	max.	Q:// ***c***	Q: // ***c***	Q: sub-// ***c***?	Q: // ***c***	Q: // ***c***
		P: // (100)	P: sub-// (001)	-	-	-
		-	T: // σ_1?	T: ?	T: sub-// ***Z***	T: sub-// ***Z***
	min.	Q: // ***a***	Q: // ***a***	Q: // ***a*** ?	Q: // basal plane	Q: // basal plane
		P: // (101)	P: // (010)	-	-	-
		-	T: sub-// ***Y***	T: sub-// ***Y***?	T: between ***X*** & ***Y***	T: sub-// ***XY***
AVs and dVs	max.	Q: // ***a***	Q: sub-// ***a***	Q: sub-// ***a***, ***c*** ?	Q: // basal plane	Q: // basal plane
		P: sub-// (110)	P: sub-// (010)	-	-	-
		-	T: sub-// ***Y***	T: sub-// ***Y*** ?	T: sub-// ***XY***	T: sub-// ***XY***
	min.	Q: // ***c***	Q: sub-// ***m*** ?	Q: sub-// ***m*** ?	Q: sub-// ***c*** & ***r***/***z*** small circle	Q: sub-// ***c*** & ***r***/***z*** small circle
		P: // (100)	P: sub-// (100), (001)?	-	-	-
		-	T: sub-// ***X*** ?	T: sub-// ***X*** ?	T: sub-// ***Z*** ?	T: sub-// ***Z*** ?

Q, quartz crystal directions (**c, m, a, r, z)**; P, plagioclase crystal directions ((100), (010), (001)); T, tectonic axes **(X≥Y≥Z)**; σ_1 and σ_3, inferred maximum and minimum principle stress directions, parallel to Q**r** (NW-SE) and Q**z** (NE-SW) respectively; //, parallel to; *note*, only shear zone wall rock contains significant plagioclase

Torridon shear zone seismic properties

The procedures described in the previous section have been applied to derive the LPO-dependent seismic properties of the Torridon mylonitic simple shear zone. In general, quartz dominates the shear zone region in terms of modal content, although plagioclase is common in the wall rock (see Fig. 1a). Thus, whilst the seismic properties of the mylonitic shear zone are likely to be derived from the quartz LPO alone, those for the wall rock represent a combination of quartz and plagioclase LPO. The relevant LPO have been combined with the single crystal elastic parameters of quartz and/or feldspar in their appropriate modal proportions, as measured by SEM/EBSD, to determine the seismic property distributions for different regions of the Torridon simple shear zone.

The first step is to derive the elastic parameters (stiffness matrix) for each region from the relevant LPO using the VRH averaging approach. Results are shown in Table 3. These data are used then to derive the seismic velocities and polarisations in three dimensions for each region by solving (2). Results are shown as stereographic projections oriented according to the sample reference frame (Fig. 6). The maximum and minimum phase velocities and anisotropy for each region, and also for single crystal quartz and feldspar (based on Fig. 4), are summarized in Fig. 7, whilst Table 4 summarizes the principle orientation relationships.

Magnitudes

The maximum and minimum velocities in Vp are fairly constant across the shear zone and range from 6.40-6.47 km/s and 5.66-5.79 km/s respectively (Figs. 6 and 7a), representing variations of only 1-2%. There is a suggestion of a slight drop in both velocities from the relatively undeformed wall rock and shear zone margin regions to the mature mylonite. However, the difference between Vp maximum and minimum values (i.e. the compressional wave anisotropy, AVp) increases from 11% in the shear zone wall rock to 12.5% in the mylonite (Figs. 6 and 7b), although the maximum value (12.8%) occurs in the

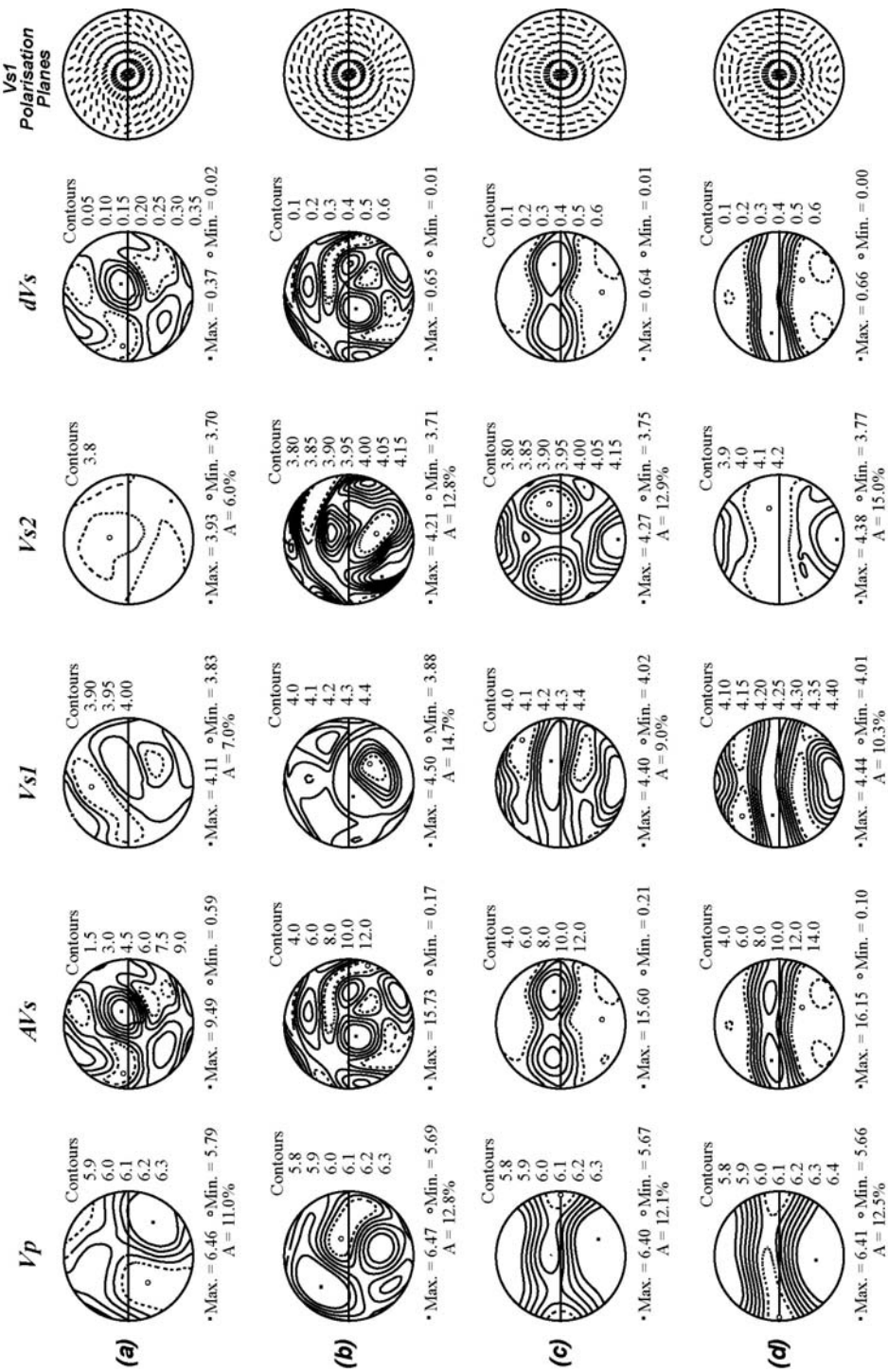

Figure 6. Seismic property distributions (Vp, Vs1, Vs2, AVs, dVs, Vs1 polarisation – see text for details) for different parts of Torridon shear zone based on LPO-averaging of elastic parameters constructed using Tables 2 and 3 and programs Anis2Ck and VpG2k (Mainprice 2003). Only shear zone wall rock includes quartz and plagioclase, the rest involve quartz alone. All pole figures equal area, upper hemispheres viewed towards ENE; contours multiples of mean uniform distribution, with tectonic X and Z directions oriented east-west and north-south respectively. See text for discussion. (a) Shear zone wall-rock (G030600). (b) Shear zone margin (G040800). (c) Mature mylonite (G270700). (d) Detail mature mylonite (G050800).

shear zone margin.

Maximum and minimum velocities in Vs1 range from 4.11-4.50 km/s and 3.83-4.02 km/s respectively, representing variations of 8.6% and 4.7% in each. The difference between Vs1 maximum and minimum values ranges from 7-

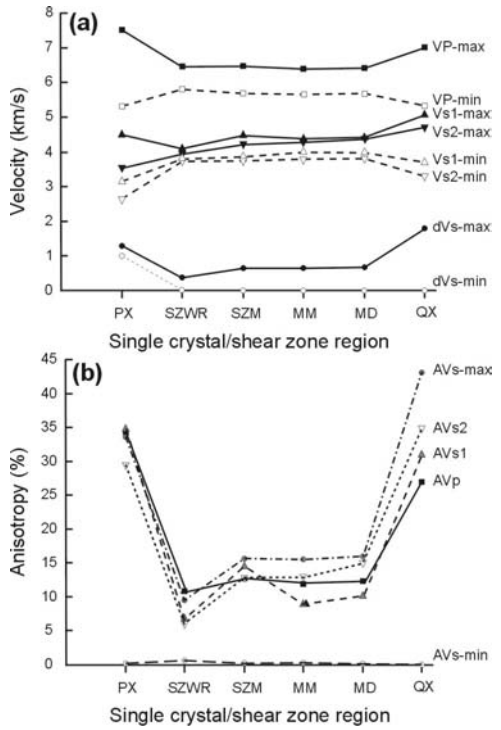

Fig. 7. Comparison of calculated variations in seismic properties (Vp, AVp, Vs1, Vs2, AVs, dVs – see text for details) for single crystal quartz (QX) and plagioclase (PX) and shear zone wall rock (SZWR), margin (SZM), mature mylonite (MM) and mylonite detail (MD) regions. See text for discussion. (a) Velocity values. (b) Anisotropy values.

15%. Maximum and minimum velocities in Vs2 range from 3.93-4.38 km/s and 3.70-3.77 km/s respectively, representing variations of 10% and 2% in each. The difference between Vs2 maximum and minimum values ranges from 4-15%. Both shear wave velocities increase from the shear zone wall rock into the margin and mature mylonite (Fig. 6 and 7a). The difference, or anisotropy, between the maximum and minimum values of Vs1 increases from 7% in the wall rock to 14.7% in the margin, before decreasing to 9-10% in the mylonite (Fig. 6 and 7b). In contrast, the anisotropy of Vs2 increases progressively from 6.0% in the wall rock to 15.0% in the mylonite.

Obviously, the behaviour of shear waves is reflected in the shear wave splitting, measured as AVs or dVs. This is typically large across the shear zone and increases from 9.49% or 0.4 km/s in the wall rock to 16.15% or 0.7 km/s in the mylonite (Figs. 6 and 7b).

Orientations

The seismic property orientation distributions, and in particular the orientations of their maximum and minimum values, relative to the LPO and tectonic reference frame are crucial in terms of explaining and using seismic properties in geodynamic interpretations (see Figs. 6 and 8, and Table 4).

The seismic property orientation distributions for the shear zone wall rock and margins regions (Fig. 6a, b) result from relatively weak LPO development (Fig. 2a, b) and, in the case of the wall rock, the contrasting impact of quartz and plagioclase LPO. Nevertheless, the seismic properties do show some consistent orientation patterns, particularly relative to the quartz LPO and tectonic reference frame. The maximum in Vp is aligned sub-parallel to the quartz ***c***-axis maximum and inferred position of σ_1, whilst the minimum in Vp is sub-parallel to the tectonic Y direction (and perhaps also the inferred position of σ_3 in the wall rock). The maximum in Vs1 has a broad distribution that encompasses the quartz ***c*** and ***r*** maximum directions, the tectonic Y direction and the inferred position of σ_1, but the orientation of the minimum in Vs1 is poorly defined relative to crystal or tectonic directions. The maximum in Vs2 aligns also sub-parallel to the quartz ***c***-axis maximum (and perhaps the inferred position of σ_1), whilst the minimum in Vs2 appears to align parallel to the quartz ***a***-axis maximum and sub-parallel to the tectonic Y direction. The orientation distributions of AVs (and dVs) have maxima oriented sub-parallel to quartz ***a***-axis concentrations and the tectonic Y direction and

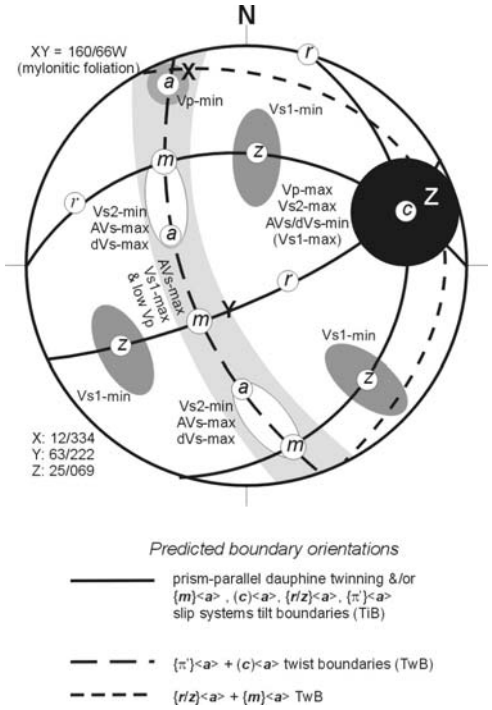

Figure 8. Summary of orientations of seismic properties (Vp, Vs1, Vs2, AVp, AVs, dVs – see text for details) with respect to Torridon shear zone tectonic (X, Y, Z) and crystallographic (quartz *c-m-a-r-z* LPO) frameworks in geographic (N) co-ordinates. Also shown are predicted orientations of principle quartz grain boundaries (Fig. 3). See text for discussion.

minima oriented sub-parallel to the tectonic X direction and perhaps quartz ***m*** direction concentrations.

In contrast to the shear zone wall rock and margin, seismic property orientation distributions in the mature mylonite are exceptionally well ordered (Fig. 6c, d) and clearly reflect the quartz LPO (Fig. 2c, d). Several of the relationships recognized in the shear zone wall rock and margin regions persist into the mylonite. A broad maximum in Vp encompasses the quartz ***c***-axis maximum and ***r***/***z*** direction small circle distributions and is sub-parallel to the tectonic Z direction. Vp has an absolute minimum parallel to the ***a***-axis maximum and tectonic X direction and a great circle distribution of low values parallel to the quartz basal plane and sub-parallel to the XY tectonic plane. Although the absolute maximum in Vs1 is sub-parallel to the tectonic Y direction, similar values occur parallel to both the quartz basal plane and the ***c***-axis maximum and hence encompass all three tectonic directions. The minima in Vs1 form small circle distributions that appear to reflect the ***r***/***z*** LPO (the absolute minimum in Vs1 may indicate the inferred directions of both σ_1 and σ_3). The maximum in Vs2 is parallel to the quartz ***c***-axis maximum and sub-parallel to the tectonic Z direction, whilst minimum values in Vs2 occupy a great circle distribution parallel to the quartz basal plane and sub-parallel to the XY tectonic plane. Maximum values in AVs and dVs occupy great circle distributions parallel to the quartz basal plane and sub-parallel to the XY tectonic plane, whilst minimum values occur over broad areas that encompass the quartz ***c***-axis maximum and ***r***/***z*** small circle distributions.

The polarisation behaviours of the fast shear waves (Vs1) for the three shear zone regions are somewhat similar, particularly for vertical wave propagation. More specifically, those for the shear zone margin rock (Fig. 6b) and the mylonite (Fig. 6c-d) are very similar.

Discussion

The results of the LPO-averaged seismic property determinations for different regions in the Torridon shear zone have significant implications for the interpretation and use of seismic velocities and anisotropy in geodynamic analysis. Firstly, it is worth comparing the single crystal seismic properties of quartz and feldspar with the LPO-averaged results obtained from the shear zone rocks to see how the former become modified in the latter. Secondly, the relationships between the LPO-averaged seismic properties and shear zone structure and tectonics are briefly considered, including the potential for using LPO-averaged seismic property results in seismic waveform modelling. Finally, the potential impact of the grain boundary microstructure elements on shear zone seismic properties is briefly considered.

Comparison between single crystal and polycrystal seismic properties

There are significant differences between the seismic properties of quartz and plagioclase single crystals and those of the three shear zone regions. The trigonal symmetry anisotropy parallel to the ***c***-axis clearly seen in single crystal quartz seismic properties (see Fig. 4a, c) is dispersed by the LPO-averaging effect in polycrystal aggregates (Fig. 6). The compressional and shear wave velocities show wider variations (higher anisotropy) for the single crystals compared to the shear zone regions (Fig. 7). This is the most important difference between single crystal and polycrystal behaviours.

In terms of orientation, the overall effect of shear zone LPO (Fig. 2) is to either displace and/or disperse (see Fig. 6 and Table 4) the unique maximum and minimum seismic orientations recognized for the single crystals (Fig. 4). For example, the sharp orientation maximum in Vp parallel to the quartz single crystal {***z***} pole becomes broadened and parallel to the ***c***-axis and/or {***z***}. Similarly, the quartz single crystal maxima in Vs1, AVs and dVs parallel to the ***a***-axes are broadened into a great circle distribution parallel to the quartz basal plane.

The polarisations of the fast shear waves (Vs1) for all three shear zone regions (Fig. 6) are very different to those of the single crystals and particularly quartz (Fig. 4c, e). This is due to the fact that although the ***c***-axes of quartz crystals are highly aligned (Fig. 2c-d), the other crystallographic directions are more dispersed in orientation. The polycrystal elasticity therefore is not trigonal in symmetry.

Relationship between shear zone structure, tectonics and seismic properties

In general, the results of the LPO-averaging of shear zone seismic properties suggests that deformation (increasing strain) during shear zone formation and mylonitisation modifies the absolute seismic velocity values and increases the seismic anisotropy of the original wall rock (Fig. 7). To consider further the relationship between shear zone structure, tectonics and seismic properties, a summary stereographic projection of the orientations (see Table 4) of structural (i.e. LPO), tectonic (i.e. X≥Y≥Z) and seismic (i.e. Vp, Vs1, Vs2, AVs, dVs) properties in the field (i.e. geographic) reference frame is shown in Fig. 8.

Recall that the mylonitic shear zone has a strong LPO (Fig. 2c, d) that approximates a dauphine twined single crystal configuration, with ***c***-axis maximum sub-parallel to Z and sub-normal to the

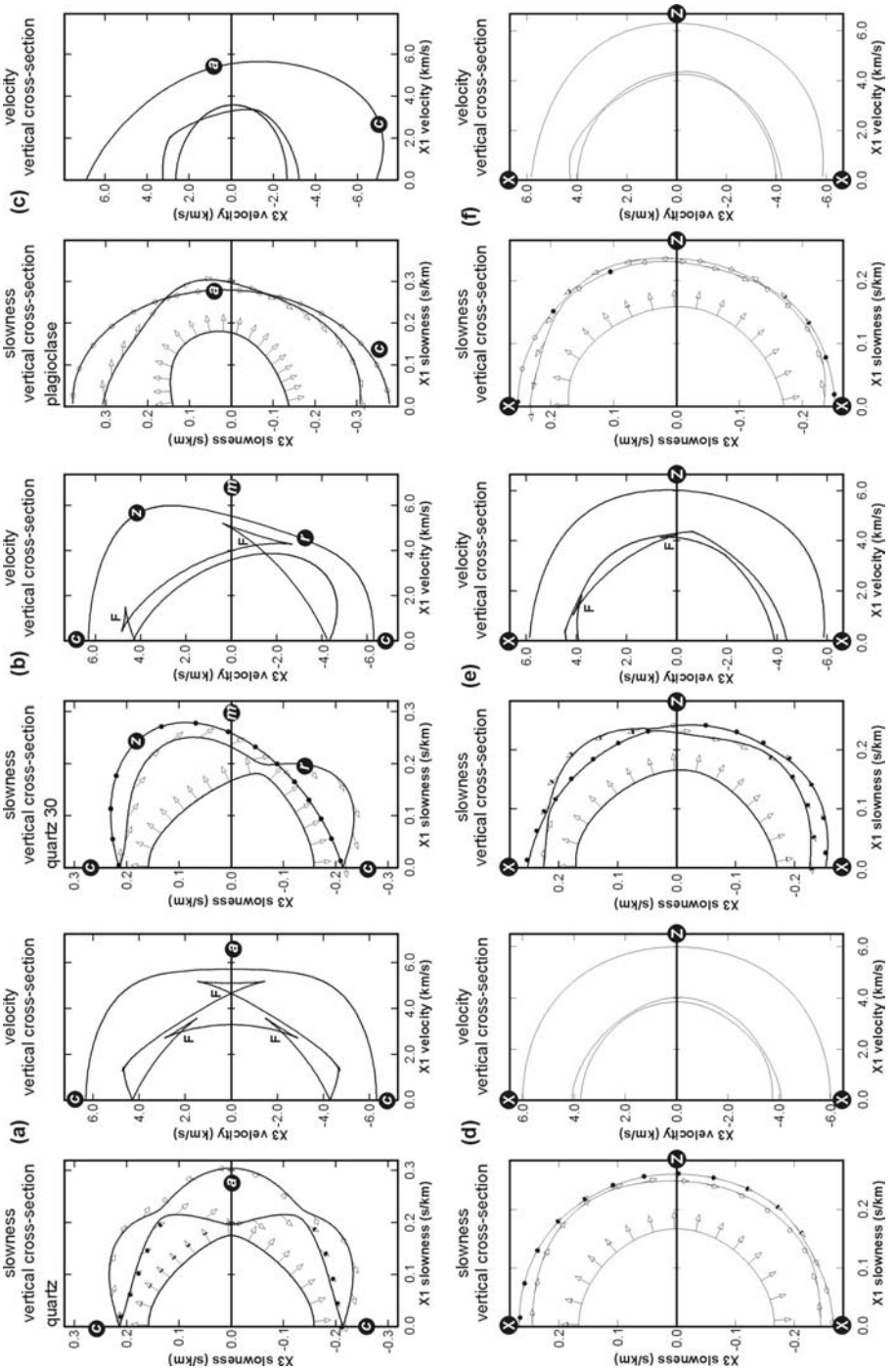

Figure 9. Cross sections through slowness and wave surfaces for single crystals and shear zone regions. In each, left-hand-side shows slowness surfaces for each wave, including directions of particle motion (arrows); note, P-wave is innermost surface. The right-hand-side shows wave surfaces and can be viewed as a snapshot of the wavefront after 1 second; note 'folding' (F) on some S-wavesheets, which is *never* seen for P-waves. (a) Quartz single crystal parallel to plane normal to ***m*** $\{10\bar{1}0\}$; note symmetry about quartz basal plane parallel to <***a***> direction. (b) Quartz single crystal parallel to plane normal to ***a*** $\{11\bar{2}0\}$; note asymmetry about quartz basal plane that reflects maximum in Vp parallel to {***z***} and minimum in Vp between {***r***} and {***m***}. (c) Plagioclase single crystal parallel to plane normal to ***b*** {010} ; note overall (triclinic) asymmetry. (d) Shear zone wall rock, XZ section. (e) Shear zone margin, XZ section (note folding). (f) Mature mylonite, XZ section.

foliation (XY) plane and ***a***-axis maximum parallel to X. The results of the LPO-averaging of the seismic properties (Figs. 6 and 7) suggest that within the mylonitic shear zone the maximum in

Vp and the minima in Vs2, AVs and dVs tend to align parallel to the ***c***-axis maximum (i.e. normal to the mylonitic foliation), whilst the minimum in Vp aligns parallel to the ***a***-axis maximum and hence defines the extension (X) direction. High values of Vs1, AVs and dVs and low values of Vp define the foliation (XY) plane, whilst the minimum in Vs1 either aligns sub-parallel to $\{z\}$ or defines a weak small circle distribution about the ***c***-axis maximum that includes $\{z\}$.

The relationships between structure, tectonics and seismic properties described above may prove useful in the tectonic interpretation of seismic measurements. However, it is clear from the geographic representation of the various parameters in Fig. 8 that any analysis of seismic waves (e.g. see below) must be interpreted in terms of the appropriate structural and tectonic orientations in the field.

Seismic waveform modelling

Wave propagation is considerably more complicated in anisotropic media than it is in isotropic media. For example, wavefronts in homogeneous anisotropic media are no longer spherical and the direction of particle motion, ray direction and wavefront normal are in general not aligned. Furthermore, two shear-waves propagate in anisotropic media and they may exhibit folding, which leads to traveltime triplications (e.g. the fast shear wave arrives at three different times at a receiver oriented parallel to the ***a***-axis of quartz, see Fig. 9a). Figure 9 illustrates these effects, showing cross-sections of the slowness and wave surfaces for the minerals and rocks of the Torridon shear-zone parallel to specific crystal (i.e. $< \bar{1}100 >$ and $< 11\bar{2}0 >$) and tectonic (i.e. XZ) planes.

It is interesting to consider how seismic waves propagate through the shear zone and how they are affected by the enhanced deformation and hence seismic anisotropy. Teleseismic and regional earthquakes provide a passive means of imaging the deep crust with relatively low frequencies and hence low resolution. In contrast, wide-angle controlled-source surveys give better resolution. Shear-wave splitting is the most unambiguous indicator of anisotropy. However, whether or not this is observable depends on the magnitude of the anisotropy and its spatial extent. The rocks of the Torridon shear-zone show varying degrees of splitting (e.g. see Figs. 6 and 7), but in general the anisotropy must be uniform and persist over a large region with respect to seismic wavelength in order to accrue a measurable level of splitting. In earthquakes studies such a region must be kilometres in extent and therefore is only likely to be observed for regional scale shear zones or rock masses with constant petrofabric characteristics (e.g. gneisses). Fortunately, reflections and mode conversions at interfaces provide better vertical resolution (perhaps 10's m for controlled source experiments) and can be very sensitive to changes in anisotropy. High degrees of anisotropy can enhance the seismic contrast across a boundary, both in terms of absolute values of anisotropy and also if the directional characteristics of the anisotropy change across the boundary.

If the crystals in the shear-zone rocks are randomly oriented, their elastic parameters are isotropic. Figure 10a, b shows the P-wave reflections and P-to-S-wave conversions at boundaries between such isotropic assemblages. These averages are based on the LPO-averaged elastic parameters for the Torridon rocks (see Tables 2, 3 and 5). The reflections are very weak, especially at near offsets (small angles of incidence).

Crystal alignment and hence anisotropy affects the reflection properties in a number of interesting ways. Figure 10c-h show the reflection coefficients for anisotropic interfaces as predicted from the petrophysical analysis described above. In general, more energy is reflected in the anisotropic case. This is due to higher vertical velocities in the underlying more-deformed layers. There is a significant level of mode-converted reflections at these interfaces. Both the fast and slow shear-waves are generated in the conversion, due to the complex anisotropic symmetries. There is a surprising amount of reflected converted-wave energy at normal incidence, which never exists in the isotropic case. This is due to the strong difference in the directions of group velocity (ray direction) and phase velocity (normal to the wavefront), again due to the low order of symmetry and strong anisotropy. There are also clear azimuthal variations in the reflections. This suggests that multi-azimuth wide-angle reflection

Table 5. *Isotropic aggregate properties of Torridon shear-zone rocks calculated from the measured elastic properties in Tables 2 and 3.*

Property	SZWR	SZM	MM
P-wave velocity (km/s)	4.298	4.291	4.290
S-wave velocity (km/s)	2.748	2.911	2.906
Density (gm/cm^3)	2.636	2.647	2.647

SZWR, shear zone wall rock; SZM, shear zone margin; MM, mature mylonite.

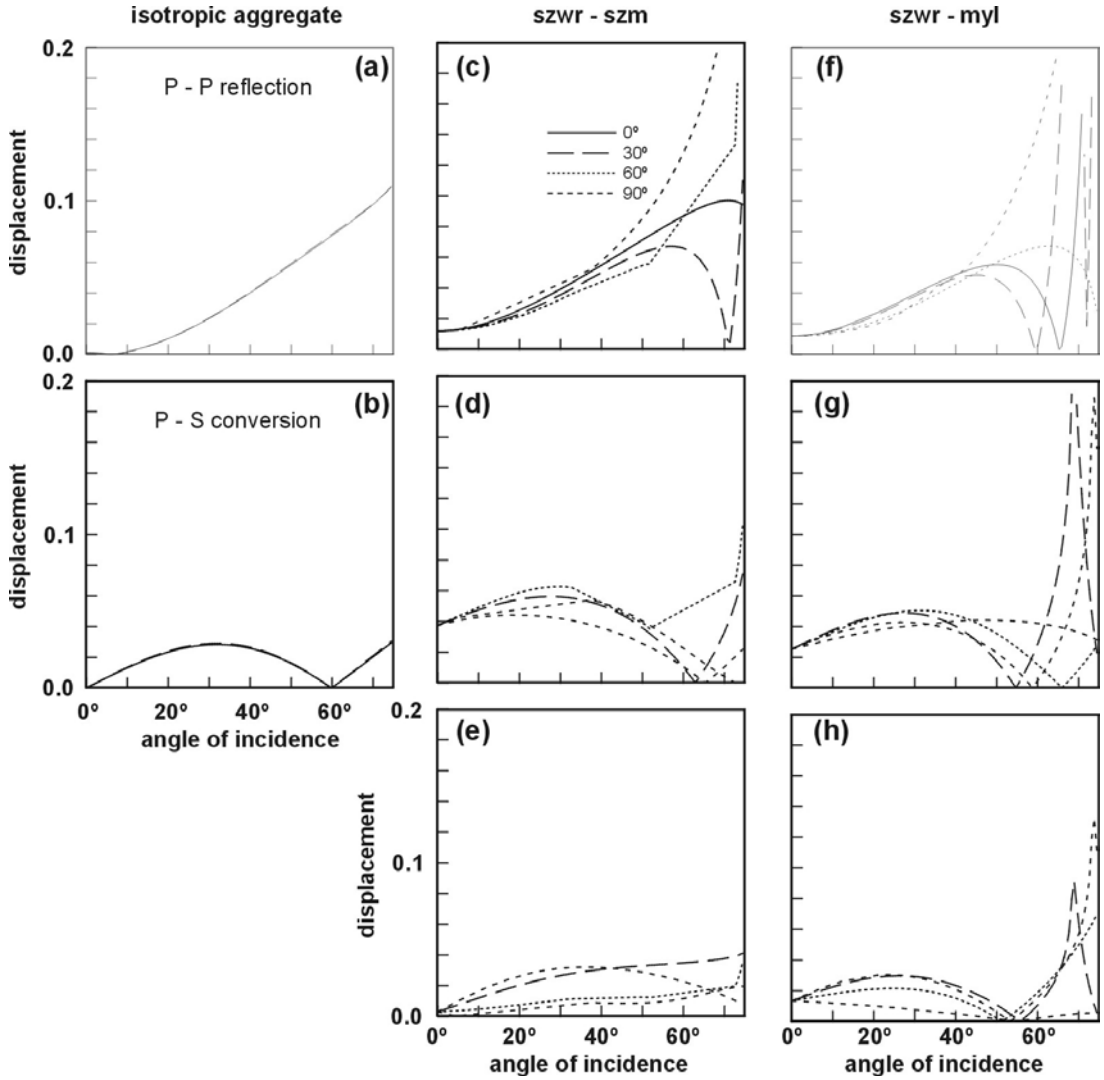

Figure 10. Seismic reflection coefficients. (a) and (b) Consider interfaces between isotropic aggregates (see Table 5) for P-wave reflections and P-S mode-converted reflections respectively. Solid line shows coefficients for isotropic shear-zone wall rock and isotropic shear-zone margin interface, whilst (barely visible) dashed line shows coefficients for interface between shear-zone wall rock and isotropic mylonite. (c) – (e) Consider an interface between anisotropic shear-zone wall rock and shear-zone margin (n.b. no azimuthal variation in reflection coefficient in isotropic cases; see (c) for key to azimuthal directions). (c) P-wave reflections as function of incidence angle and azimuthal angle. (d) Mode-converted reflections for P-S1-waves. (e) Mode-converted reflections for P-S2-waves. (f) – (h) Consider an interface between anisotropic shear-zone wall rock and mature mylonite (n.b. no azimuthal variation in reflection coefficient in isotropic cases; see (c) for key to azimuthal directions). (f) P-wave reflections as function of incidence angle and azimuthal angle. (g) Mode-converted reflections for P-S1-waves. (h) Mode-converted reflections for P-S2-waves.

data can be potentially used to study the sense of deformation in deep-rooted shear zones (see also Burlini et al. 1998; Khazanehdari et al. 1998). Such reflection effects have been used also to map fracture patterns in oil reservoirs (Hall and Kendall 2003).

Grain boundary microstructure

In addition to LPO, a number of other microstructural elements are known to impact on elastic anisotropy, such as cracks, fractures, pores, grain morphology and shape preferred orientation, and layering. The impact of many of these elements on elastic anisotropy has recently been considered by Wendt et al. (2003) and further discussion here is largely inappropriate. However, it is worth considering one particular microstructural element, the role of grain boundaries, that impacts directly on the present study.

Grain boundaries are important microstructural elements in rocks and may contribute a significant volume fraction, particularly in fine grained rocks such as mylonites. They represent regions of relatively high lattice distortion and defect concentration that form extended three-dimensional

networks and are likely to have different elastic parameters from those of the grains. In addition, as rock elasticity is dependent also on cohesion forces between grains (Kaarsberg, 1959), the contact area between grains should be considered. Furthermore, grain boundaries may form crack-like discontinuities in some rocks and consequently influence seismic anisotropy if the boundaries are preferentially aligned (e.g. Babuska and Cara, 1991). Thus, many rock properties, including the elastic parameters, may be influenced by the grain boundary network.

Unfortunately, there is little known about the exact impact of grain boundaries on seismic anisotropy (e.g. Wendt et al. 2003). However, a recent interpretation of the microstructural and petrofabric evolution of the Torridon shear zone (Lloyd *in press*) considered the formation and orientation of quartz grain boundaries. It was suggested that the grain boundary network consists of tilt boundaries parallel to quartz prism (and hence often YZ tectonic) planes and twist boundaries parallel to the XY foliation/basal-crystal planes and XZ tectonic plane (see Fig. 3). The *physical* presence of grain boundaries was not considered in the LPO-averaging analysis described here and hence any *direct* impact due to grain boundary configuration on seismic properties can not be assessed. However, comparison between grain boundary and seismic property orientations (Fig. 8; see also Fig. 6) may provide significant indications, as follows.

Twist boundaries that developed parallel to the XY foliation/basal crystal planes due to a combination of {***π'***}<***a***> + (***c***)<***a***> slip could contribute to the great circle distribution of high AVs, dVs and Vs1 and low Vp values. In addition, the broad concentration of high/maximum Vp, Vs2 and Vs1 and low/minimum AVs and dVs values parallel to the quartz ***c***-axis maximum and sub-parallel to the tectonic Z direction may be influenced by two characteristics of the grain boundary network: 1. the intersection of tilt boundaries that develops due to a combination of dauphine twinning and/or slip on systems that exploit the quartz <***a***> axis as the slip direction; and 2 twist boundaries that develop parallel to the XZ tectonic plane due to combined slip on {***r/z***}<***a***> + {***m***}<***a***> systems. Similarly, the tendency for the minimum in Vp to occur parallel to the quartz ***a***-axis maximum and sub-parallel to the tectonic X direction may be augmented by the intersection of twist boundaries that develop parallel to the XY foliation/basal crystal planes and XZ tectonic plane due to combined slip on {***π'***}<***a***> + (***c***)<***a***> and {***r/z***}<***a***> + {***m***}<***a***> systems respectively. Thus, it appears that grain boundary configuration has the *potential* to impact on seismic property characteristics but much further work (i.e. direct measurements) is needed.

Conclusions

This contribution has explored the link between petrofabric (LPO) and petrophysical (seismic) properties of a quartzo-feldspathic shear zone developed under conditions typical of the mid-lower crust. Although it is clear that shear zone formation and petrofabric evolution from an initially quartzo-feldspathic gneissic wall rock to a mature quartz mylonite is reflected in the seismic properties, the precise impact of LPO on seismic properties is not simple. Several conclusions can be drawn, based on these observations.

(1) The most obvious control of LPO on shear zone seismic properties results in the following relationships: Vp-min parallel to the ***a***-maximum (i.e. tectonic X); AVs-max parallel to mylonitic foliation (i.e. XY mylonitic foliation plane); Vp-max and AVs-min parallel the ***c***-maximum (i.e. foliation normal, Z); and Vs1-min parallel to the ***z***-maxima.

(2) The development of a strong LPO during shear zone evolution, and particularly during mylonitisation, is responsible for considerable seismic anisotropy. P-wave anisotropy varies between 11-13%, the fast and slow shear-waves show 6-15% anisotropy, and the magnitude of shear-wave splitting is 9.5-16%.

(3) Although the degree of shear wave splitting exhibited by the shear zone due to LPO requires considerable thicknesses of rock (depending on the dominant wavelength of the source) with constant LPO characteristics before it becomes seismically visible, reflections and mode conversions provide much better resolution, particularly across boundaries (e.g. between the shear zone margin and the mature mylonite).

(4) The low symmetry and strong anisotropy due to the petrofabric suggest that multi-azimuth wide-angle reflection data may be useful in the determination of the deformation characteristics of deep shear zones.

(5) How well seismic data can be ultimately used to study anisotropy and hence lower crustal deformation remains to be seen. Data quality and spatial coverage will be crucial.

We thank David Mainprice for use of his LPO and seismic property calculation and plotting programs. The original manuscript was considerably improved by the comments of two anonymous referees. Part of the automated EBSD system used was funded by UK N.E.R.C. Grant GR9/3223 (GEL).

References

ALEKSANDROV, K.S., ALCHIKOV, U.V., BELIKOV, B.P., ZASLAVSKI, B.I. AND KRUPNYI, A.I. 1974. Velocities of elastic waves in minerals at atmospheric pressure and increasing precision of elastic constants by means of EVM. *Izv. Acad. Sci. USSR Geol. Ser*. **10**, 15-24.

BABUSKA, V. AND CARA, M. 1991. Seismic Anisotropy in the Earth. Kluwer Academic, Dordrecht.

BASCOU, J., BARRUOL, G., VAUCHEZ, A. MAINPRICE, D. AND EGYDIO-SILVA, M. 2001. EBSD-measured lattice preferred orientations and seismic properties of eclogites. *Tectonophysics* **342**, 61-80.

BLACKMAN, D.K., WENK, H-R. AND KENDALL, J-M. 2002. Seismic anisotropy of the upper mantle: 1, Factors that affect mineral texture and effective elastic properties. Geochem., Geophys. Geosystems 3, 8601, doi:10.1029/2001GC000248, 2002.

BUNGE, H.J. 1982. Texture Analysis in Materials Science. Butterworths, London, 599pp.

BUNGE, H.J., KIEWEL, R., REINERT, TH. AND FRITSCHE, L. 2000. Elastic properties of polycrystals – influence of texture and stereology. *Journal of the Mechanics and Physics of Solids* **48**, 29-66.

BURLINI, L. AND KERN, H. 1994. Special Issue: Seismic properties of crustal and mantle rocks - Laboratory measurements and theoretical calculations. *Surveys in Geophysics* **15**, 439-672.

BURLINI, L. AND KUNZE, K. 2000. Fabric and seismic properties of Carrara marble mylonite. *Physics & Chemistry of the Earth* **25**, 133-139.

BURLINI, L., MARQUER, D., CHALLANDES, N., MAZZOLA, S. AND ZANGARINI, N. 1998. Seismic properties of highly strained marbles from the Splugenpass, central Alps. *Journal of Structural Geology* **20**, 277-292.

CASEY, M. 1981. Numerical analysis of X-ray textural data - an implementation in FORTRAN allowing triclinic or axial specimen symmetry and most crystal symmetries. *Tectonophysics* **78**: 51-64.

CHRISTENSEN, N.I. 1966. Elasticity of ultrabasic rocks. *Journal of Geophysical Research* **71**, 5921-5931.

CROSSON, R.S. AND LIN, J.W. 1971. Voigt and Reuss prediction of anisotropic elasticity of dunite. *Journal of Geophysical Research* **76**, 570-578.

DANA, E.S. AND FORD, W.E. 1951. A Textbook of Mineralogy. John Wiley and Sons.

DINGLEY, D.J. 1984. Diffraction from sub-micron areas using electron backscattered diffraction in a scanning electron microscope. *Scanning Electron Microscopy* **2**, 569-575.

HALL, S. AND KENDALL, J-M. 2003. Fracture characterisation at Valhall: application of P-wave AVOA analysis to a 3D ocean-bottom data set. *Geophysics* **68**, 1150-1160.

HESS, H.H. 1964. Seismic anisotropy of the uppermost mantle under oceans. *Nature* **203**, 629-631.

HILL, R. 1952. The elastic behaviour of a crystalline aggregate. *Proceedings of the Physical Society, London A* **65**, 351-354.

JI, S., WANG, Q. AND XIA, B. 2002. Handbook of Seismic Properties of Minerals, Rocks and Ores. Polytechnic International Press, Canada.

KAARSBERG, E.A. 1959. Introductory studies of natural and artificial argillaceous aggregates by sound-propagation and X-ray diffraction methods. *Journal of Geology* **67**, 447-472.

KENDALL, J-M. 2000. Seismic anisotropy in the boundary layers of the Earth's mantle. In: Karato, S-I., Forte, A.M., Lieberman, R.C., Masters, G., Stixrude, L. (Eds) Earth's deep interior; mineral physics and tomography from the atomic to the global scale. *Geophysical Monograph* **117**, 149-175.

KERN, H. 1982. P- and S-wave velocities in crustal and mantle rocks under the simultaneous action of high confining pressure and high temperature and the effect of microstructure. In: Schreyer, W. (ed.), High Pressure Researches in Geoscience. H. Schweizerhart'sche Verlagsbuchhandlung, Stuttgart, 15-45.

KERN, H. AND WENK, H-R. 1985. Anisotropy in rocks and the geological significance. In: Wenk, H-R. (Ed.) Preferred orientation in deformed metals and rocks: an introduction to modern texture analysis, Academic Press, Orlando, 537-555.

KHAZANEHDARI, J., RUTTER, E.H., CASEY, M. AND BURLINI, L. 1998. The role of crystallographic fabric in the generation of seismic anisotropy and reflectivity of high strain zones in calcite rocks. *Journal of Structural Geology* **20**, 293-300.

LAW, R.D., SCHMID, S.M. AND WHEELER, J. 1990. Simple shear deformation and quartz crystallographic fabrics - a possible natural example from the Torridon area of NW Scotland. *Journal of Structural Geology* **12**, 29-45.

LISTER, G.S. AND SNOKE, A. 1984. S-C mylonites. *Journal of Structural Geology* **6**, 617-638.

LLOYD, G.E. 1987. Atomic number and crystallographic contrast images with the SEM: a review of backscattered electron techniques. *Mineralogical Magazine* **51**, 3-19.

LLOYD, G.E. 2000. Grain boundary contact effects during faulting of quartzite: an SEM/EBSD analysis. *Journal of Structural Geology* **22**, 1675-1693.

LLOYD, G.E. Microstructural evolution in a mylonitic quartz simple shear zone: the significant roles of dauphine twinning and misorientation. In: Alsop, G.I., Holdsworth, R.E., McCaffrey, K. and Hand, M. (eds) Transports and Flow Processes in Shear Zones, Geological Society, London Special Publications, *in press*.

LLOYD, G.E., LAW, R.D., MAINPRICE, D. AND WHEELER, J. 1992. Microstructural and crystal fabric evolution during shear zone formation. *Journal of Structural Geology* **14**, 1079-1100.

MAINPRICE D. 1990. An efficient Fortran program to calculate seismic anisotropy from the lattice preferred orientation of minerals. *Computers and Geosciences* **16**,385-393.

MAINPRICE, D. 2003. World Wide Web Address: http://www.isteem.univ-montp2.fr/TECTONOPHY/petrophysics/software/petrophysics_software.html.

MAINPRICE, D. AND HUMBERT, M. 1994. Methods of calculating petrophysical properties from lattice preferred orientation data. *Survey Geophysics* **15**, 575-592.

MAINPRICE, D. AND SILVER, P.G. 1993. Interpretation of SKS waves using samples from the subcontinental lithosphere. *Physics of Earth and Planetary Interiors* **78**, 257-280.

MAINPRICE, D., LLOYD, G.E. AND CASEY, M. 1993. Individual orientation measurements in quartz polycrystals - advantages and limitations for texture and petrophysical property determinations. *Journal of Structural Geology* **15**, 1169-1187.

MAINPRICE, D., BARRUOL, G. AND BEN ISMAIL, W. 2000. The seismic anisotropy of the Earth's mantle; from single crystal to polycrystal. In: Karato, S-I., Forte, A.M., Lieberman, R.C., Masters, G., Stixrude, L. (Eds) Earth's deep interior; mineral physics and tomography from the atomic to the global scale. Geophysical Monograph **117**, 237-264.

MAINPRICE, D., POPP, T., GUEGUEN, Y., HUENGES, E., RUTTER, E.H., WENK, H-R. AND BURLINI, L. 2003. Physical Properties of Rocks and other Geomaterials, a Special Volume to honour Professor H. Kern. *Tectonophysics* **370**, 1-311.

MAULER, A., BURLINI, L., KUNZE, K., BURG, J.P. AND PHILIPPOT, P. 2000. P-wave anisotropy in eclogites and relationship to omphacite crystallographic fabric. *Physics and Chemistry of the Earth* **25**, 119-126.

MCSKIMIN, H.J., ANDREATCH, JR., P., AND THURSTON, R.N. 1965. Elastic moduli of quartz versus hydrostatic pressure at 25°C and -195.8°C. Journal of Applied Physics 36, 1624-1632.

NYE, J.F. 1957. Physical properties of crystals. Clarendon press, Oxford. 322p.

PESELNICK, L.A., NICOLAS, A. AND STEVENSON, P.R. 1974. Velocity anisotropy in a mantle peridotite from the Ivrea Zone: application to upper mantle anisotropy. *Journal of Geophysical Research* **79**, 1175-1182.

PRIOR, D.J., BOYLE, A.P., BRENKER, F., CHEADLE, M.C., DAY, A., LOPEZ, G., POTTS, G.J., REDDY, S., SPIESS, R., TIMMS, N., TRIMBY, P. WHEELER, J. AND ZETTERSTROM, L. 1999. The application of electron backscatter diffraction and orientation contrast imaging in the SEM to textural problems in rocks. *American Mineralogist* **84**, 1741-1759.

PROS, Z., LOKAJICEK, T, PRIKRYL, R. AND KLIMA, K. 2003. Direct measurement of 3D elastic anisotropy on rocks from the Ivrea zone (Southern Alps, NW Italy). *Tectonophysics* **370**, 31-47.

RAMSAY, J.G. 1980. Shear zone geometry: a review. *Journal of*

Structural Geology **2**, 83-100.
RAMSAY, J.G. & GRAHAM, R.H. 1970. Strain variation in shear belts. *Canadian Journal of Earth Sciences* **7**, 786-813.
REUSS, A. 1929. Berechnung der Fließgrenze von Mischkristallen auf Grund der Plastizitätsbedingungen fur Einkristalle. *Zeitschrift für Angewandte Mathematik und Mechanik* **9**, 49-58.
SCHMIDT, N.H. AND OLESEN. N.Ø. 1989. Computer-aided determination of crystal-lattice orientation from electron channelling patterns in the SEM. *Canadian Mineralogist* **27**, 15-22.
SERONT, B., MAINPRICE, D. AND CHRISTENSEN, N.I. 1993. A determination of the three dimensional seismic properties of anorthosite: comparison between values calculated from the petrofabric and direct laboratory measurements. *Journal of Geophysical Research* **98**, 2209-2221.
SINOGEIKIN, S.V. AND BASS, J.D. 2000. Single-crystal elasticity of pyrope and MgO to 20 GPa by Brillouin scattering in the diamond cell. *Physics of the Earth and Planetary Interiors* **120**, 43-62.
VENABLES, J.A. AND HARLAND, C.J. 1973. Electron backscattering patterns - a new technique for obtaining crystallographic in formation in the scanning electron microscope. *Philosophical Magazine* **27**, 1193-1200.
VOIGT, W. 1928. Lehrbuch der Kristallphysik: mit Ausschluss der Kristalloptik. B.G. Teubner, Leipzig. 978p.
WENDT, A.S., WIRTH, R., BAYUK, I.O., COVEY-CRUMP, S.J. AND LLOYD, G.E. 2003. An Experimental and Numerical Study of the Microstructural Parameters Contributing to the Seismic Anisotropy of Rocks. *Journal of Geophysical Research* 108(B8), 2365, doi:10.1029/2002JB001915.
WHEELER, J. 1984. A new plot to display the strain of elliptical markers. *Journal of Structural Geology* **6**, 417-423.